Sample preparation and zircon extraction at UC Davis:

Sample preparation for zircon extraction at UC Davis involves: 1) washing the sample with soap and warm water, 2) crushing the rock with a combination of a hydraulic press (if needed), mortar/pestle, and Bico Pulverizer, 3) sieving to the preferred size fraction (generally <250 um for detrital zircon samples, 63-125 um for igneous zircon samples), 4) heavy mineral concentration by decanting and panning, 5) magnetic separation using a Frantz isodynamic separater, 6) density separation with Lithium Polytungstate. These steps usually result in a sufficiently pure zircon separate. However, additional steps are sometimes required to further concentrate zircon. These steps include: 7) additional panning, 8) density separation with Methylene Iodide, 9) acid wash to dissolve pyrite. Once the mineral separate is sufficiently pure, zircon grains are mounted by pouring the detrital the zircon concentrate onto sticky tape or by picking for igneous zircon analysis.

Mounting:

Once the desired zircon separate is obtained, we mount the zircons in epoxy. This involves pressing double-sided sticky tape on a flat glass plate and placing (or pouring) the zircon grains and reference materials on the tape. Once grains are mounted, we submerge them en epoxy, which is contained by a 1" diameter plastic cylinder. After curing, the epoxy cylinder is removed from the sticky tape and ground/polished until the zircon interiors are exposed.

Imaging:

We image all zircon grains and standards prior to analysis by LA-ICP-MS. Our imaging protocol makes use of the Cameca SX-100 electron microprobe housed in the Earth and Planetary Sciences department at UC Davis. We image the zircon grains using the 'high-gain' electron beam setting on the Cameca SX-100. By adjusting the brightness and contrast of the backscattered electron (BSE) image, the high gain beam reveals internal zoning structure of the zircon grains. Increasing the scan rate on these BSE images yields a high-resolution greyscale image of the zircon crystal and its internal zoning structure. For igneous or metamorphic zircon analyses, we image each individual crystal and use the high-resolution BSE images to choose our laser spots prior to analysis. We also use the Cameca SX-100 to measure the width of metamorphic growth rims, which helps us determine whether or not it will yield a reliable U-Pb date. For detrital analyses, we use the high-gain beam with a moderate scan rate. This approach still displays zoning features of the zircon grain interior, but at a decreased resolution, which allows imaging of an entire detrital mount in a reasonable timeframe (generally less than 1.5 hr). We image the detrital grain mounts using the 'Video map' feature of the Cameca SX-100. This feature images user-designated domains of the mount in series and then stiches the images together into a rasterized image of the entire grain mount. The end result is a moderate resolution, high contrast image of all grains on the 1" epoxy round. We print all zircon images for igneous, metamorphic, and detrital analyses prior to LA-ICP-MS analysis and mark the printed images during the laser session.

U-Pb zircon data collection with the Element2 HR ICPMS at the ALC:

U-Pb geochronology of zircons is conducted by laser ablation inductively coupled plasma mass spectrometry (LA-ICPMS) at the Arizona LaserChron Center (ALC) (Gehrels et al., 2006, 2008; Gehrels and Pecha, 2014). The analyses involve ablation of zircon with a Photon Machines Analyte G2 excimer laser equipped with HelEx ablation cell using a spot diameter of 20 microns.

The ablated material is carried in helium into the plasma source of an Element2 HR ICPMS, which sequences rapidly through masses corresponding to U, Th, and Pb isotopes. Signal intensities are measured with an SEM that operates in pulse counting mode for signals less than 50K cps, in both pulse-counting and analog mode for signals between 50K and 5M cps, and in analog mode above 5M cps. The calibration between pulse-counting and analog signals is determined line-by-line for signals between 50K and 5M cps, and is applied to >5M cps signals. Four intensities are determined and averaged for each isotope, with dwell times that are listed in Table S1.1.

With the laser set at an energy density of ~5 J/cm2, a repetition rate of 8 hz, and an ablation time of 10 seconds, ablation pits are ~12 microns in depth. Sensitivity with these settings is approximately ~5,000 cps/ppm. Each analysis consists of 5 sec on peaks with the laser off (for backgrounds), 10 sec with the laser firing (for peak intensities), and a 20 second delay to purge the previous sample and save files.

Table S1.1: Instrument settings and data processing at Arizona LaserChron Center

Analytical Settings for U-Pb Geochronology at the Arizona LaserChron Center (Element 2 Single Collector)	
Laboratory and Sample Preparation	
Laboratory name	Arizona LaserChron Center
Sample type/mineral	Zircon
Sample preparation	Conventional mineral separation, 1 inch epoxy mount, polished to 1-micron finish
Imaging	Hitachi 3400N SEM with BSE and/or Cathodoluminesence
Laser ablation system	
Make, Model, and type	Photon Machines Analyte G2 Excimer laser
Ablation cell and volume	HelEx ablation cell
Laser wavelength	193 nm
Pulse width	~8 ns
Energy density	~7 J/cm2
Repetition rate	8 Hz
Alation duration	10 s
Ablation pit depth/ablation rate	~12 microns & 0.8 microns/sec
Spot diameter nominal/actual	20 microns
Sampling mode/pattern	Spot
Carrier gas	Helium

Cell carrier gas flow	0.11 L/min He in inner cup, 0.29 L/min He in cell
ICP-MS instrument	
Make, Model, and type	Thermo Element2 HR ICPMS
Sample introduction	Ablation aerosol
RF power	1200 W
Make-up gas flow	0.8 L/min Ar
Detection system	Dual mode Secondary Electron Multiplier
Masses measured	202Hg, 204(Hg+Pb), 206Pb, 207Pb, 208Pb, 232Th, 235U, 238U
Dwell times (ms)	202=5.2, 204=7.8, 206=20.2, 207=28.4, 208=2.6, 232=2.6, 235=15.4, 238=10.4
Total integration time per output data point (sec)	202=1.5, 204=2.3, 206=5.9, 207=8.3, 208=7.6, 232=7.6, 235=4.5, 238=3.0
Sensitivity as useful yield	~5000 cps/ppm
IC dead time	22 ns
Data processing	
Gas blank	8 sec on-peak zero subtracted
Calibration strategy	SLM zircon used as primary standard
Reference material information	Gehrels et al. (2008)
Data processing package used/Correction for LIEF	E2agecalc
Mass discrimination	Normalized to primary standard
Common Pb correction, composition and uncertainty	Common Pb correction based on measured 206Pb/204 Pb and the assumed composition of common Pb based on Stacey and Kramers (1975)
Uncertainty level and propagation	Uncertainties for individual analyses propagated at 1-sigma. Uncertainty of pooled analyses propagated at 2-sigma.
Quality control/validation	FC-1 and R33 analyzed as secondary standards.
Other information	Primary and secondary standards mounted together with unknowns.
	Analytical methods described by Gehrels et al. (2008), Gehrels and Pecha (2014), and Pullen et al. (2018)

U-Pb data reduction methods at the ALC:

Following analysis, data reduction is performed with an in-house Python decoding routine and an Excel spreadsheet (E2agecalc) that:

1. Decodes .dat files from the Thermo software such individual intensities for measurement are available (routine written by John Hartman, University of Arizona)

2. Imports intensities and a sample name for each analysis

3. Calculates average intensities for each isotope (based on the sum of all counts while the laser is firing)

4. Subtracts ^{204}Hg from the 204 signal to yield ^{204}Pb intensity (using natural ^{202}Hg/^{204}Hg of 4.3). This Hg correction is not significant for most analyses because our Hg backgrounds are low (generally ~150 cps at mass 204).

5. Performs a common Pb correction based on the measured ^{206}Pb/^{204}Pb and the assumed composition of common Pb based on Stacey and Kramers (1975)

6. Calculates measured 206/238, 206/207, and 208/232 ratios

7. Compares measured and known ratios for the three standards to determine fractionation factors for 206/238, 206/207, and 208/232. These correction factors are generally <5% for 206/238, <2% for 206/207, and <20% for 208/232.

8. Determines an overdispersion factor if the standard analyses show greater dispersion than expected from measurement uncertainties

9. Uses a sliding-window average to apply fractionation factors to unknowns (generally averaging 8 standard analyses)

10. Calculates fractionation-corrected 206/238, 206/207, and 208/232 ratios and ages for unknowns

11. Propagates measurement uncertainties for 206/238 and 208/232 that are based on the scatter about a regression of measured values. Uncertainties for 206/207 and 206/204 are based on the standard deviation of measured values since these ratios generally do not change during an analysis. The sum of this uncertainty and any overdispersion factor is reported as the internal (or measurement) uncertainty for each analysis. These uncertainties are reported at the 1-sigma level.

12. Calculates the down-hole slope of 206/238 to highlight analyses in which 206/238 is compromised due to heterogeneity in age (e.g., crossing an age boundary) or intersection of a fracture or inclusion.

13. Calculates concentrations of U and Th for unknowns based on the measured intensity and known concentrations of FC-1.

14. Calculates the external (systematic) uncertainties for 206/238, 206/207, and 208/232, which include contributions from (a) the scatter of standard analyses, (b) uncertainties in the ages of the standards, (c) uncertainties in the composition of common Pb, and (4) uncertainties in the decay constants for ^{235}U and ^{238}U.

15. Determines a "Best Age" for each analysis, which is generally the 206/238 age for <900 Ma ages and the 206/207 age for >900 Ma ages.

16. Provides preliminary filters that highlight analyses with >20% discordance, >5% reverse discordance, or >10% internal (measurement) uncertainty.

17. Corrects 206/238U ages for U-Th disequilibrium. This has a significant impact only on very young (~<2 Ma) ages.

18. Calculates the radiation dosage that the analyzed portion of each zircon has experienced, assuming a value of 2.3 for the Th/U of the magma. This is plotted against 206/238 age to help identify Pb loss.

18. Creates a publication-ready datatable with concentrations, isotope ratios, and ages for unknowns.

U-Pb zircon data collection with the LA-Q-ICP-MS at UC Davis:

U-Pb geochronology of zircon is conducted by laser ablation quadrupole inductively coupled plasma mass spectrometry (LA-Q-ICP-MS) at UC Davis. The analyses involve ablation of zircon with a Photon Machines Analyte G2 excimer laser equipped with HelEx ablation cell using a spot diameter of 25 microns. The ablated material is carried in helium into the plasma source of an Agilent 7700 Series Q-ICP-MS, which sequences rapidly through masses corresponding to U, Th, Pb, and Hg isotopes. Dwell times for each of these masses are listed in Table S1.2.

Instrument settings on the LA-Q-ICP-MS system at UC Davis are based on a published calibration using nearly identical equipment (Matthews and Guest, 2017). Matthews and Guest (2017) used optical profilometry to measure a pit depth of ~12 um using the laser settings listed in Table S1.2. Since we used the instrument settings published by Matthews and Guest (2017), we infer that the analyses performed at UC Davis result in a laser pit depth of ~12 um. Uranium sensitivity with these settings is approximately ~230 cps/ppm, which we approximate using the NIST 610 glass. Each analysis consists of 15 sec on peaks with the laser off (for backgrounds) and 15 sec with the laser firing (for peak intensities),

Table S1.2: Instrument settings and data processing at UC Davis

Laboratory & Sample Preparation	
Laboratory name	Dept. of Earth and Planetary Sciences, UC Davis
Sample type/mineral	Zircon U-Pb detrital and igneous
Sample preparation	Conventional mineral separation, 1 inch resin mount, 1μm polish to finish
Imaging	BSE images Cameca SX-100 electron microprobe
Laser ablation system	
Make, Model & type	Photon Machines Analyte G2 Excimer Laser
Ablation cell & volume	HelEx ablation cell
Laser wavelength (nm)	193 nm
Pulse width (ns)	~8 ns
Fluence ($J.cm^{-2}$)	1.88 $J.cm^{-2}$
Repetition rate (Hz)	10 Hz
Ablation duration (secs)	15 s
Ablation pit depth / ablation rate	~12μm pit depth, inferred from Mathews and Guest (2017).
Spot diameter (μm) nominal/actual	25 μm / ~30 μm, square aperture
Sampling mode / pattern	Static spot ablation
Carrier gas	Helium
Cell carrier gas flow (l/min)	0.75
ICP-MS Instrument	
Make, Model & type	Agilent 7700 series Q-ICP-MS
Sample introduction	Ablation aerosol
RF power (W)	1350W
Make-up gas flow (l/min)	1.1
Detection system	Electron Multiplier
Masses measured	91, 201, 202, 204, 206 207, 235, 238
Integration time per peak/dwell times (s); quadrupole settling time between mass	0.01, 0.01, 0.01, 0.03, 0.04, 0.07, 0.015, 0.015, 0.02 s. In order of masses listed above.

jumps	
Total integration	0.239 s
'Sensitivity' as useful yield	~230 cps/ppm U Estimated on NIST 610 glass
IC Dead time (ns)	
Data Processing	
Gas blank	15 second on-peak zero subtracted
Calibration strategy	FC-1 used as primary reference material, R-33 used as secondary/validation
Reference Material info	FC-1 (Paces and Miller, 1993; Schmitz et al., 2003) R-33 (Black et al. 2004)
Data processing package used / Correction for LIEF	Iolite-Igor data reduction scheme based on methods of Paton et al, (2010) and Petrus and Kamber (2012). Laser-Induced Elemental Fractionation correction assumes reference material and samples behave identically.
Mass discrimination	$^{206}Pb/^{238}U$ additionally normalized to reference material
Common-Pb correction, composition and uncertainty	No common-Pb correction applied to the data.
Uncertainty level & propagation	Ages are quoted at 2*s* absolute, propagation is by quadratic addition. Reproducibility and age uncertainty of reference material are propagated where appropriate.
Quality control / Validation	FC-1 and R-33 natural zircon reference materials
Other information	

U-Pb data reduction methods at UC Davis:

Data from the Q-ICP-MS are imported into Igor Pro-Iolite and displayed as a time series. Integration periods for gas blanks (backgrounds), standards, and unknowns are selected manually. FC-1 (Paces and Miller, 1993; Schmitz et al., 2003) is used as the primary reference material and R-33 (Black et al., 2004) is used as a secondary reference. Estimates of elemental concentrations, and thus U/Th, are also determined using FC-1. Isotope ratios, dates, and associated uncertainties are calculated from the integrations using the *U_Pb_geochronology3* data reduction scheme (Paton et al., 2010). After initial dates are calculated, we use the *Live Concordia* feature of the *VizualAge* data reduction scheme (Petrus and Kamber, 2012) to screen each integration period for discordance related to inclusions and/or mixed age domains (e.g., a spurious date resulting from ablating through a younger rim into an older core). If an analysis is found to be discordant apparently related to the aforementioned causes, we conservatively adjust the integration interval to obtain the most reliable date at reasonable uncertainty. Once screened, we export the data, 2s internal and external uncertainties, and elemental concentrations. We

report our data using the datatable template suggested by Horstwood et al. (2016), which may be found at www.Plasmage.org.

It is important to convey that the Agilent 7700 Q-ICP-MS at UC Davis is not currently equipped with a Hg trap in the carrier gas line. This results in generally high background ^{204}Hg. Although we monitor mass 204 (Hg + Pb) during analysis sessions, the elevated background 204 signal precludes determination of meaningful ^{204}Pb/^{206}Pb ratios. Thus, we do not apply any common Pb correction to the data. However, we do consider the 204 signal during integration periods. If the 204 signal is elevated above background levels during ablation of a zircon, it is likely indicating the presence of ^{204}Pb. Due to the assumptions and high level of uncertainty that would be introduced by attempting to do a common Pb correction on such analyses, we reject analyses on grains that display elevated 204 relative to the background gas blank. Such rejections are uncommon.

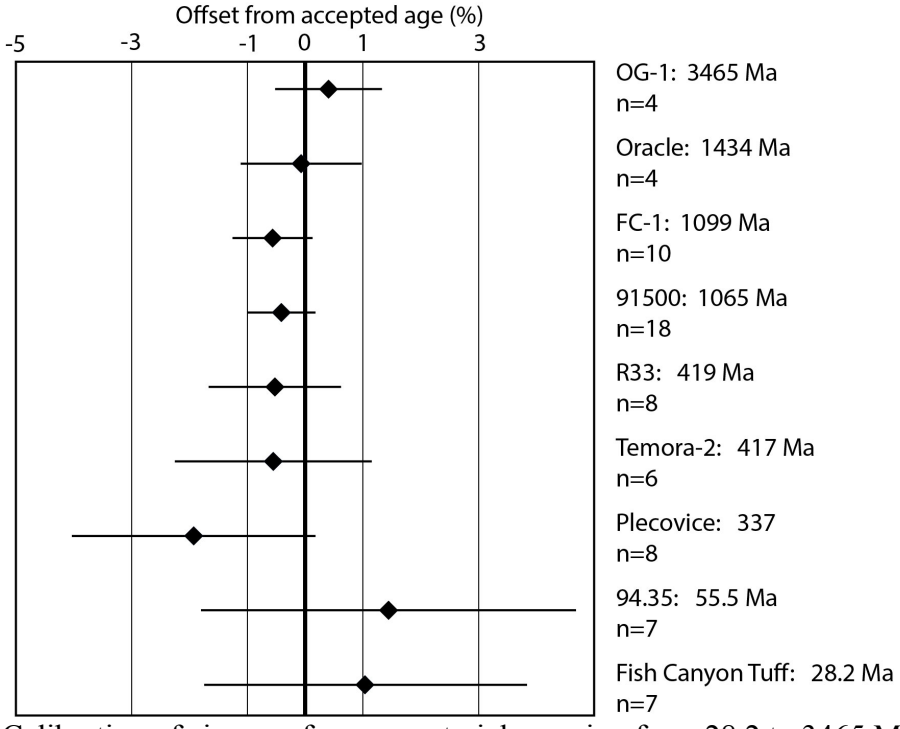

Figure S1.1: Calibration of zircon reference materials ranging from 28.2 to 3465 Ma using the LA-Q-ICP-MS at UC Davis. All analyses were performed using the ablation settings described above. Each diamond represents multiple analyses on multiple grains (n=number of analyses) during a single session.

Data filtering methods:

We parsed the single grain dates from both labs using Tera-Wasserburg concordia diagrams, U/Th ratios, and zoning patterns.

Reverse discordance- Single grain analyses from some of our samples suffered from reverse discordance. Because the causes of reverse discordance are not well understood, but may result either from heterogeneous distribution of U- and Pb-rich zones in a crystal (Danisik et al., 2017), or the partial dissolution of U-rich zones by fluids (Mattinson et al., 1996), we filtered our U-Pb dates to exclude those which are reverse discordant and do not overlap within uncertainty of the concordia curve. The ^{206}Pb/^{238}U dates from the reverse discordant grains generally overlap with

$^{206}Pb/^{238}U$ dates of concordant or normally discordant analyses. Yet, the $^{207}Pb/^{206}Pb$ ages are either very young, or in some cases, negative (i.e., future ages). Because the reverse discordant analyses come from samples that experienced upper greenschist to amphibolite facies conditions and several grains from these samples show textures indicating partial dissolution, we interpret the reverse discordant analyses as the result of interaction with corrosive fluids. Thus, we reject these analyses from the detrital population, despite the overlap in $^{206}Pb/^{238}U$ dates.

≤900 Ma detrital grain dates are used in KDE plots if the $^{206}Pb/^{238}U$ date has an uncertainty (2s internal) of <10% and <u>either</u> of the following criteria are met:

1. The 2s internal uncertainty ellipse intersects the concordia curve on a Tera-Wasserburg diagram, allowing the concordia curve to account for decay constant uncertainties.
2. The date is discordant, but the $^{207}Pb/^{206}Pb$ date is <3 times the $^{206}Pb/^{238}U$ date.

≥900 Ma detrital grain dates are used in KDE plots if <u>both</u> of the following criteria are met:

1. The date is <5% reverse discordant
2. The date is <20% normally discordant

Dates are interpreted to record post-depositional metamorphic recrystallization if the grain was recovered from a metamorphic rock that experienced appropriate temperatures to recrystallize zircon (estimated petrographically using mineral assemblages) and <u>one or more</u> of the following criteria are met:

1. The date overlaps with the known age of cross cutting intrusive rocks within the map unit.
2. The dated grain, or region of the grain, lacks internal zoning, which is suggestive of metamorphic recrystallization (Hoskin and Schaltegger, 2003).
3. The analysis targeted an overgrowth rim identified in BSE images.
4. The U/Th ratio of the analysis is elevated (>20) and/or variable within the population of dates.

Dates (as part of a population) are used to calculate metamorphic or igneous ages if <u>all</u> of the following criteria are met:

1. The 2s internal uncertainty ellipse intersects the concordia curve on a Tera-Wasserburg diagram, allowing the concordia curve to account for decay constant uncertainties.
2. The $^{206}Pb/^{238}U$ date has <10% uncertainty (2s internal) (For igneous analyses only).
3. Isoplot does not reject the date during the weighted mean calculation.

For populations of igneous or metamorphic grain dates, ages are calculated using the weighted mean function in Isoplot (Ludwig, 2008). Following the protocol of Horstwood et al. (2016), only 2s internal uncertainties are used in the weighted mean calculation and systematic uncertainties are added quadratically to the internal uncertainty after the weighted mean is calculated. Uncertainties on igneous or metamorphic ages reported in the main text include both internal (included in weighted mean calculation) and systematic (added on after weighted mean calculation) unless otherwise indicated.

Maximum depositional ages are estimated to be the mean age of the youngest statistical population of detrital dates (Herriott et al., 2019).

REFERENCES CITED

Black, L.P., Kamo, S.L., Allen, C.M., Davis, D.W., Aleinikoff, J.N., Valley, J.W., Mundil, R., Campbell, I.H., Korsch, R.J., Williams, I.S., and Foudoulis, C., 2004, Improved $^{206}Pb/^{238}U$ microprobe geochronology by the monitoring of a trace-element-related matrix effect; SHRIMP, ID–TIMS, ELA–ICP–MS and oxygen isotope documentation for a series of zircon standards: Chemical Geology, v. 205, no. 1–2, p. 115–140, https://doi.org/10.1016/j.chemgeo.2004.01.003.

Danišík, M., McInnes, B.I., Kirkland, C.L., McDonald, B.J., Evans, N.J., and Becker, T., 2017, Seeing is believing: Visualization of He distribution in zircon and implications for thermal history reconstruction on single crystals: Science Advances, v. 3, no. 2, p. e1601121, https://doi.org/10.1126/sciadv.1601121.

Gehrels, G., and Pecha, M., 2014, Detrital zircon U-Pb geochronology and Hf isotope geochemistry of Paleozoic and Triassic passive margin strata of western North America: Geosphere, v. 10, no. 1, p. 49–65, https://doi.org/10.1130/GES00889.1.

Gehrels, G., Valencia, V., and Pullen, A., 2006, Detrital zircon geochronology by laser-ablation multicollector ICPMS at the Arizona LaserChron Center: The Paleontological Society Papers, v. 12, p. 67–76, https://doi.org/10.1017/S1089332600001352.

Gehrels, G.E., Valencia, V., and Ruiz, J., 2008, Enhanced precision, accuracy, efficiency, and spatial resolution of U-Pb ages by laser ablation-multicollector-inductively coupled plasma-mass spectrometry: Geochemistry Geophysics Geosystems, v. 9, Q03017, https://doi.org/10.1029/2007GC001805.

Herriott, T.M., Crowley, J.L., Schmitz, M.D., Wartes, M.A., and Gillis, R.J., 2019, Exploring the law of detrital zircon: LA-ICP-MS and CA-TIMS geochronology of Jurassic forearc strata, Cook Inlet, Alaska, USA: Geology, v. 47, no. 11, p. 1044–1048, https://doi.org/10.1130/G46312.1.

Horstwood, M.S., Košler, J., Gehrels, G., Jackson, S.E., McLean, N.M., Paton, C., Pearson, N.J., Sircombe, K., Sylvester, P., Vermeesch, P., and Bowring, J.F., 2016, Community-derived standards for LA-ICP-MS U-(Th-) Pb geochronology–Uncertainty propagation, age interpretation and data reporting: Geostandards and Geoanalytical Research, v. 40, no. 3, p. 311–332, https://doi.org/10.1111/j.1751-908X.2016.00379.x.

Hoskin, P.W., and Schaltegger, U., 2003, The composition of zircon and igneous and metamorphic petrogenesis: Reviews in mineralogy and geochemistry: Zircon: v. 53(1), p. 27–62.

Ludwig, K., 2008, Isoplot 3.6: Berkeley Geochronology Center Special Publication 4, 77 p.

Matthews, W.A., and Guest, B., 2017, A practical approach for collecting large-n detrital zircon U-Pb data sets by quadrupole LA-ICP-MS: Geostandards and Geoanalytical Research, v. 41, no. 2, p. 161–180, https://doi.org/10.1111/ggr.12146.

Mattinson, J.M., Graubard, C.M., Parkinson, D.L., and McClelland, W.C., 1996, U-Pb reverse discordance in zircons: the role of fine-scale oscillatory zoning and sub-micron transport of Pb: Geophysical Monograph-American Geophysical Union, v. 95, p. 355–370, https://doi.org/10.1029/GM095p0355.

Paces, J.B., and Miller, J.D., Jr., 1993, Precise U-Pb ages of Duluth complex and related mafic intrusions, northeastern Minnesota: Geochronological insights to physical, petrogenetic, paleomagnetic, and tectonomagmatic processes associated with the 1.1 Ga midcontinent rift system: Journal of Geophysical Research. Solid Earth, v. 98, B8, p. 13997–14013, https://doi.org/10.1029/93JB01159.

Paton, C., Woodhead, J.D., Hellstrom, J.C., Hergt, J.M., Greig, A., and Maas, R., 2010, Improved laser ablation U-Pb zircon geochronology through robust downhole fractionation correction: Geochemistry Geophysics Geosystems, v. 11, no. 3, https://doi.org/10.1029/2009GC002618.

Petrus, J.A., and Kamber, B.S., 2012, VizualAge: A novel approach to laser ablation ICP-MS U-Pb geochronology data reduction: Geostandards and Geoanalytical Research, v. 36, no. 3, p. 247–270, https://doi.org/10.1111/j.1751-908X.2012.00158.x.

Pullen, A., Ibanez-Mejia, M., Gehrels, G., Giesler, D., and Pecha, M., 2018, Optimization of a Laser Ablation-Single Collector-Inductively Coupled Plasma-Mass Spectrometer (Thermo Element 2) for Accurate, Precise, and Efficient Zircon U-Th-Pb Geochronology: Geochemistry Geophysics Geosystems, v. 19, https://doi.org/10.1029/2018GC007889.

Schmitz, M.D., Bowring, S.A., and Ireland, T.R., 2003, Evaluation of Duluth Complex anorthositic series (AS3) zircon as a U-Pb geochronological standard: New high-precision isotope dilution thermal ionization mass spectrometry results: Geochimica et Cosmochimica Acta, v. 67, no. 19, p. 3665–3672, https://doi.org/10.1016/S0016-7037(03)00200-X.

Stacey, J.S., and Kramers, J.D., 1975, Approximation of terrestrial lead isotope evolution by a two stage model: Earth and Planetary Science Letters, v. 26, p. 207–221, https://doi.org/10.1016/0012-821X(75)90088-6.